Latin American Journal of Solids and Structures
www.lajss.org

Physical and geometrical non-linear analysis of plane frames considering elastoplastic semi-rigid connections by the positional FEM

Abstract

This study presents an alternative Finite Element formulation based on positions to model plane frames considering geometrical non-linear and elastoplastic behavior for members and semi-rigid connections. The formulation includes shear effects and allows the consideration of important mechanical behavior of structures in design decisions and verifications. The principle of stationary energy is used to find the equilibrium equations. A multi-linear elastoplastic constitutive law is developed for both continuum members and semi-rigid connections in order to comprise any proposed stress-strain diagram. Large rotations and displacements are considered for both semi-rigid connections and structure. The most important steps used to derive the formulation are described along the paper and various examples are used to validate and show the possibilities of the proposed technique.

Keywords

Frames, Physical and geometrical non-linear analysis, Positional FEM, Elastoplastic connections, Laminate cross sections.

Marcelo Campos Junqueira Reis[a]
Humberto Breves Coda[a, *]

[a] Structural Engineering Department, Escola de Engenharia de São Carlos, Universidade de São Paulo

[*] Author e-mail: hbcoda@sc.usp.br

1 INTRODUCTION

Computational technology improvements provide a continuous advance in structural analysis, resulting in designs of lighter and slender structures. In this sense, the geometrical and physical non-linear analysis of structures, including any kind of flexible connection, acquire special importance in engineering analysis. From this reasoning it is necessary to develop a well-posed non linear formulation allowing the accurate evaluation of displacements and efforts of conventional and unconventional structures.

Various researches related to geometrical non linear analysis of two and three-dimensional frames that consider plasticity can be cited. Some pioneering authors as Shi and Atluri (1988) and Argyris et al (1982) applied co-rotational techniques to analyze three-dimensional frames developing plasticity. In these works elastoplasticity were treated in a discrete way (plastic hing-

es), in which a moment-curvature relation is assumed for continuous members cross sections. One can cite some recent works that follows the same localized plastic hinge strategy to model the behavior of frame elements, are they: Zhou and Chan (2004), Ren et al (1999), Armero and Ehrlich (2006), Ehrlich and Armero (2005), White (1993), Chen et al (1996), Landesmann and Batista (2005), Chan and Zhou (2004) and Ngo-Huu et al (2007).

Some authors as Alvarenga and Silveira (2009), Avery and Mahendran (2000) and Gruttmann et al (2000) use distributed plasticity to model two and three dimensional frames. One advantage of distributed plasticity, when compared to plastic hinges, is the better representation of the plastic evolution over cross sections, without the necessity of a previous knowledge of moment-curvature curves. However, both plastic hinges and the existent distributed plasticity frame models do not consider the shear stress influence as the finite element proposed in this work.

Concerning problems in which semi-rigid connections are present one can cite the works of Lui and Chen (1988), King (1994), Simões (1996), Chui and Chan (1997), Xu (2001), Sekulovic and Salatic (2001), Pinheiro (2003), Kruger et al. (1995) and Chan and Chui (2000). All these works use second order geometrical description, which limits the range of applications, i.e., displacements and rotations should not be large.

In order to implement semi-rigid connections in any computational code it is necessary to use results from works that study the experimental behavior of these connection, as, for example, Chen and Kishi (1989) and Abdalla and Chen (1995). Some works that, using experimental results, try to establish empirical mathematical models for connections behavior are also present in literature see, for example, the works of Richard and Abbott (1975), Frye and Morris (1975), Ang and Morris (1984), Lui and Chen (1986), Lui and Chen (1988), Kishi and Chen (1986a), Kishi and Chen (1986b) and Zhu et al. (1995). In our work, as an alternative to these empirical formulas, we propose a multi-linear elastoplastic diagram that allows to follow the experimental results for semi-rigid connections. Moreover the elastoplastic behavior ensures realistic results for cycling loads that are not provided by the non-linear elastic empirical formulas proposed by the previously mentioned works.

In the present work an alternative position based Finite Element (FE) formulation (Bonet et al., 2000 and Coda and Greco, 2004) is developed to comprise geometrical and physical non-linearity of both frame members and connections. The formulation, originally developed and presented in this work, is geometrically exact and, considering the Reissner kinematic hypothesis, includes shear stress contribution in both displacement and failure criterion. Based on Botta et al. (2008), the developed elastoplastic algorithm is multi-linear with an alternative flow direction rule, which allow the reproduction of any stress-strain curve and the determination of closed solution for the plastic multiplier. Moreover, semi-rigid elastoplastic connections develop large rotations allowing realistic analysis of unload situations for which connections and/or frame elements suffers plastic deformations.

We start the formulation description by defining the Reissner kinematic for laminate frame elements passing through the establishment of the total potential energy including plastic dissipation for both frame elements and semi-rigid connections. After that, the principle of stationary energy is employed to write the equilibrium equations (regarding positions) and the elastoplastic evolution is defined. The Newton-Raphson procedure is used to solve the non-linear system of

equations and examples are presented to validate the proposed formulation and to show its possibilities.

2 FRAME ELEMENT REISSNER KINEMATICS

The FE formulation presented here is called positional as it is based on positions, not displacements (Bone et al., 2000 and Coda and Greco, 2004). The main advantage of this total lagrangian strategy is the establishment of the gradient deformation without the explicit use of the chain rule (Coda and Paccola, 2008, Coda, 2009 and Coda and Paccola, 2010). The chain rule operation appears as a simple numerical matrix inversion, which allows the generalization of this procedure for any class of non-linear mechanical problem (Coda and Paccola, 2010, Coda and Paccola, 2011, Nogueira et. al., 2012, Silva and Coda, 2013 and Pascon and Coda, 2013).

In this section we present the complete development of the alternative 2D positional Reissner kinematics to be used in the proposed finite element formulation.

2.1 Initial configuration

The positional formulation is based on two mappings, one related to the initial configuration and another related to the current configuration. To describe the initial configuration mapping one starts with the reference line approximation, see Figure 1, by the following expression:

$$f_{oi}^{m}(\xi) = x_i^m(\xi) = \phi_\ell X_{i\ell}^m \tag{1}$$

in which i is the coordinate direction (1 or 2), m represents the reference line and ℓ the element node (or shape function). In expression (1) the repetition of index ℓ indicates summation (Einstein notation). Figure 1 shows 4 nodes (cubic approximation), however any quantity of nodes or approximation order may be chosen.

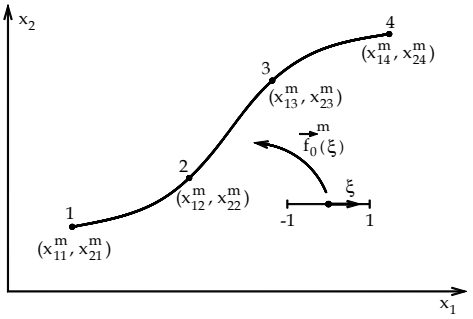


Figure 1 Reference line parameterization for initial configuration (cubic approximation)

In Figure 1 $f_0^m(\xi)$ is the mapping from the non-dimensional variable ξ to the reference line. A similar mapping from the non-dimensional variable to the current reference line will be given in the next item.

We start to build the initial configuration of the frame element writing an approximation for the normal vector, Figure 2, using the known initial reference line mapping, as follows:

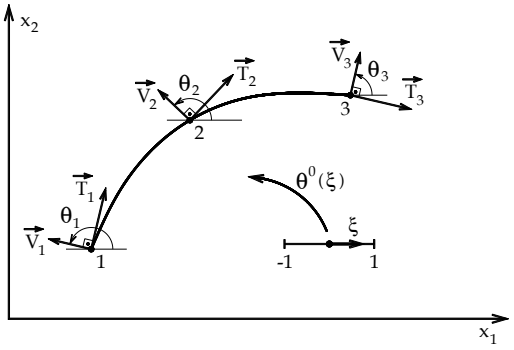


Figure 2 Nodal normal vectors

The tangent vector at any point of the reference line can be written, particularly at nodes, by:

$$T_{ik} = \left.\frac{d\phi_\ell(\xi)}{d\xi}\right|_{\xi_k} X^m_{i\ell} \tag{2}$$

in which ξ_k is non-dimensional coordinate of node k and T_{ik} is the i_{th} component of the tangent vector at node k.

As a consequence, if the coordinates of reference line nodes are known, the tangent vectors at nodes are also known and the normal vectors can by calculated as:

$$V_{1k} = -T_{2k} / \sqrt{T_{i(k)} T_{i(k)}} \tag{3}$$

$$V_{2k} = T_{1k} / \sqrt{T_{i(k)} T_{i(k)}} \tag{4}$$

in which index inside brackets does not mean summation, that is:

$$\sqrt{T_{i(k)} T_{i(k)}} = \sqrt{(T_{1(k)})^2 + (T_{2(k)})^2} \tag{5}$$

For the present positional formulation it is important to write the nodal angle θ_k that the normal vector V_{ik} makes with the horizontal direction (x_1 axis), see Figure 2, as:

$$\theta^0_k = arctg(V_{2(k)} / V_{1(k)}) \tag{6}$$

Knowing the nodal angles we use the same shape functions to approximate $\theta^0(\xi)$ along the initial configuration:

$$\theta^0(\xi) = \phi_\ell(\xi)\theta^0_\ell \tag{7}$$

Observing Figure 3 one can find any point inside the continuum (frame) adding the normal vector $g_i^0(\xi,\eta)$ to a point of the reference line, as:

$$x_i(\xi,\eta) = x_i^m(\xi) + g_i^0(\xi,\eta) \tag{8}$$

in which η is the second non-dimensional variable used to build the 2D frame element.

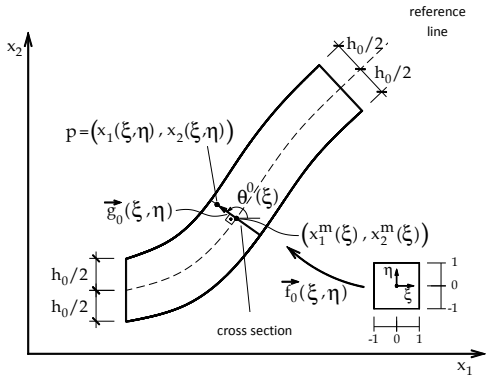


Figure 3 Point P at a general cross section of the initial element configuration

Moreover, vector $g_i^0(\xi,\eta)$ generates cross sections with (in this paper) constant height h_0. The width is also considered constant (b_0) along the bar length, however it can vary along transverse direction to compose general cross sections. This transverse variation is opportunely introduced.

From Figure 3 it is established that the initial cross section is orthogonal to the reference line, so vector $g_i^0(\xi,\eta)$ can be written as a function of $\theta^0(\xi)$, as follows:

$$g_1^0(\xi,\eta) = \frac{h_0}{2}\eta\cos(\phi_\ell(\xi)\theta^0_\ell) \tag{9}$$

$$g_1^0(\xi,\eta) = \frac{h_0}{2}\eta\, sen(\phi_1(\xi)\theta^0_1) \tag{10}$$

in which η varies from -1 to $+1$.

Substituting equations (9), (10) and (1) into (8) results the complete mapping from (ξ,η) to the initial configuration of a frame element, as:

$$f_{01}(\xi,\eta) = x_1(\xi,\eta) = \phi_\ell X_{1\ell}^m + \frac{h_0}{2}\eta\cos(\phi_\ell(\xi)\theta_\ell^0) \tag{11}$$

$$f_{02}(\xi,\eta) == x_2(\xi,\eta) = \phi_\ell X_{2\ell}^m + \frac{h_0}{2}\eta sen(\phi_\ell(\xi)\theta_\ell^0) \tag{12}$$

2.2 Current configuration:

The necessary information to build the initial configuration comprises the reference line nodal coordinates, the height and the width of the cross section. The current configuration is achieved by a non-linear process that uses a trial position to start the solution procedure. So, we do not worry at this moment about the solution process and writes the current configuration similarly to the initial one, that is:

$$f_{11}(\xi,\eta) = y_1(\xi,\eta) = \phi_\ell Y_{1\ell}^m + \frac{h_0}{2}\eta\cos(\phi_\ell(\xi)\theta_\ell) \tag{13}$$

$$f_{12}(\xi,\eta) = y_2(\xi,\eta) = \phi_\ell Y_{2\ell}^m + \frac{h_0}{2}\eta sen(\phi_\ell(\xi)\theta_\ell) \tag{14}$$

For which y_i are the current coordinates of a general point inside the frame element, $Y_{i\ell}^m$ are current nodal coordinates and θ_ℓ are the current angles of cross sections, see Figure 4.

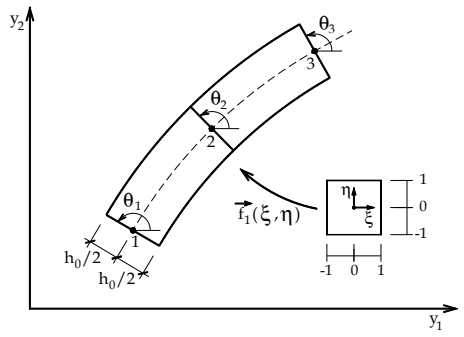


Figure 4 Current configuration mapping – detaching angles

One can see from Figure 4 and from equations (13) and (14) that cross sections remain straight, but no more orthogonal to the reference line. This is the general Reissner kinematics. Moreover we kept h_0 and b_0 unchanged limiting our constitutive relation to accept any shear elastic modulus, but null Poisson ratio.

2.3 Change of configuration function (deformation) and its gradient:

Being defined mappings to initial and current configurations, we start the description of the change of configuration of the analyzed body (frame). This is done by joining the two mappings of Figures 3 and 4 in a single representation, see Figure 5, for which the function $\vec{f}$ describes the change of configuration from initial configuration (B_0) to the current one (B). From basic knowledge of calculus $\vec{f}$ is written as a composition of mappings $\vec{f}_0$ and $\vec{f}_1$ as:

$$\vec{f} = \vec{f}_1 \circ (\vec{f}_0)^{-1} \tag{15}$$

and the gradient of $\vec{f}$, called here $\mathbf{A}$ (a 2x2 tensor) is written from the gradient of $\vec{f}_0$ and $\vec{f}_1$ as:

$$\mathbf{A} = \mathbf{A}^1 \cdot (\mathbf{A}^0)^{-1} \tag{16}$$

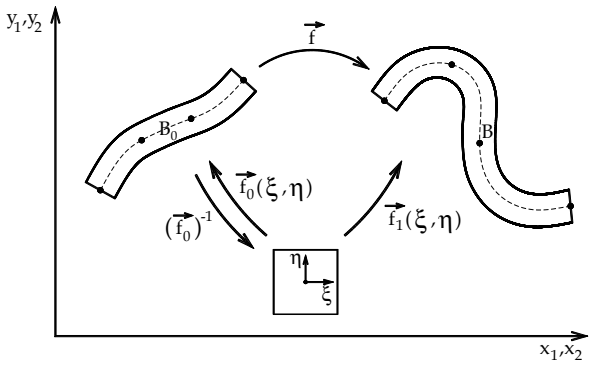


Figure 5 – Change of configuration – Positional mapping

In index notation one writes

$$A_{ij} = A_{ik} D_{jk} \tag{17}$$

in which D_{kj} is the inverse of A^0_{kj}.

These gradients are written in an open form as:

$$A^0_{ij} = \begin{bmatrix} \dfrac{\partial f^0_1}{\partial \xi} & \dfrac{\partial f^0_1}{\partial \eta} \\ \dfrac{\partial f^0_2}{\partial \xi} & \dfrac{\partial f^0_2}{\partial \eta} \end{bmatrix} = \begin{bmatrix} \dfrac{\partial x_1}{\partial \xi} & \dfrac{\partial x_1}{\partial \eta} \\ \dfrac{\partial x_2}{\partial \xi} & \dfrac{\partial x_2}{\partial \eta} \end{bmatrix} \tag{18}$$

$$A_{ij}^{1}=\begin{bmatrix} \dfrac{\partial f_1^1}{\partial \xi} & \dfrac{\partial f_1^1}{\partial \eta} \\ \dfrac{\partial f_2^1}{\partial \xi} & \dfrac{\partial f_2^1}{\partial \eta} \end{bmatrix}=\begin{bmatrix} \dfrac{\partial y_1}{\partial \xi} & \dfrac{\partial y_1}{\partial \eta} \\ \dfrac{\partial y_2}{\partial \xi} & \dfrac{\partial y_2}{\partial \eta} \end{bmatrix} \tag{19}$$

Elements of A_{ij}^{0} and A_{ij}^{1} are calculated directly from expressions (11), (12), (13) and (14) for known values (integration points) of ξ and η, as:

$$A_{11}^{0}=\frac{\partial x_1}{\partial \xi}=\phi_{\ell,\xi}(\xi)X_{1\ell}^{m}-\frac{h_0}{2}\eta sen(\phi_\ell(\xi)\theta_\ell^0)\phi_{k,\xi}(\xi)\theta_k^0 \tag{20}$$

$$A_{12}^{0}=\frac{\partial x_1}{\partial \eta}=\frac{h_0}{2}\cos(\phi_\ell(\xi)\theta_\ell^0) \tag{21}$$

$$A_{21}^{0}=\frac{\partial x_2}{\partial \xi}=\phi_{\ell,\xi}(\xi)X_{2\ell}^{m}+\frac{h_0}{2}\eta\cos(\phi_\ell(\xi)\theta_\ell^0)\phi_{k,\xi}(\xi)\theta_k^0 \tag{22}$$

$$A_{22}^{0}=\frac{\partial x_2}{\partial \eta}=\frac{h_0}{2}sen(\phi_\ell(\xi)\theta_\ell^0) \tag{23}$$

$$A_{11}^{1}=\frac{\partial y_1}{\partial \xi}=\phi_{\ell,\xi}(\xi)Y_{1\ell}^{m}-\frac{h_0}{2}\eta sen(\phi_\ell(\xi)\theta_\ell)\phi_{k,\xi}(\xi)\theta_k \tag{24}$$

$$A_{12}^{1}=\frac{\partial y_1}{\partial \eta}=\frac{h_0}{2}\cos(\phi_\ell(\xi)\theta_\ell) \tag{25}$$

$$A_{21}^{1}=\frac{\partial y_2}{\partial \xi}=\phi_{\ell,\xi}(\xi)Y_{2\ell}^{m}+\frac{h_0}{2}\eta\cos(\phi_\ell(\xi)\theta_\ell)\phi_{k,\xi}(\xi)\theta_k \tag{26}$$

$$A_{22}^{1}=\frac{\partial y_2}{\partial \eta}=\frac{h_0}{2}sen(\phi_\ell(\xi)\theta_\ell) \tag{27}$$

The objective Green-Lagrange strain measure $\boldsymbol{E}$ is chosen to develop the geometrically exact FEM, that is:

$$\mathbf{E}=\frac{1}{2}(\mathbf{C}-\mathbf{I})=\frac{1}{2}(\mathbf{A}^{t}\mathbf{A}-\mathbf{I}) \text{ or } E_{ij}=\frac{1}{2}(A_{ki}A_{kj}-\delta_{ij}) \tag{28}$$

where $\mathbf{I}$ is the second order identity tensor and $\mathbf{C}$ is the right Cauchy stretch.

In order to introduce lamina with different widths and material properties, one should simply change expressions (11), (12), (13) and (14) by:

$$x_1(\xi,\eta)=\phi_\ell X_{1\ell}^m+\left(d_{lam}+\frac{h_0^{lam}}{2}\eta\right)\cos(\phi_\ell(\xi)\theta_\ell^0) \tag{29}$$

$$x_2(\xi,\eta)=\phi_\ell X_{2\ell}^m+\left(d_{lam}+\frac{h_0^{lam}}{2}\eta\right)sen(\phi_\ell(\xi)\theta_\ell^0) \tag{30}$$

$$y_1(\xi,\eta)=\phi_\ell Y_{1\ell}^m+\left(d_{lam}+\frac{h_0^{lam}}{2}\eta\right)\cos(\phi_\ell(\xi)\theta_\ell) \tag{31}$$

$$y_2(\xi,\eta)=\phi_\ell Y_{2\ell}^m+\left(d_{lam}+\frac{h_0^{lam}}{2}\eta\right)sen(\phi_\ell(\xi)\theta_\ell) \tag{32}$$

in which d_{lam} is the distance between the reference line and the concerned lamina following the positive sense of the vector defined by θ, see Figure 3. It is worth noting that h_0^{lam} is the height of each lamina. Moreover, it is necessary to indicate the width b_{lam} and the physical properties of each lamina at an integration point for which the constitutive model and the deformation gradient are required.

It is important to stress that distortion effects are naturally considered resulting in a general Reissner-Mindlin kinematics.

3 ELASTIC PROCEDURE

In this section, the elastic Saint-Venant-Kirchhoff constitutive relation is adopted to relate the second Piola-Kirchhoff stress $\boldsymbol{S}$ and the Green strain $\boldsymbol{E}$ for frame elements. Moreover, semi-rigid linear elastic connections are introduced to make a preliminary development of the complete non-linear solution technique to be shown in the next section.

3.1 Elastic connections:

In order to unify the notation, the degree of freedom θ_ℓ will be called $Y_{3\ell}$. Each element node has three degrees of freedom, but when connecting elements by means of semi-rigid connections (global numbering) an extremity node may have more than three degrees of freedom, as the rotations of the connected elements are not the same. Figure 6 shows three cases to illustrate the linking by means of free connections (joints).

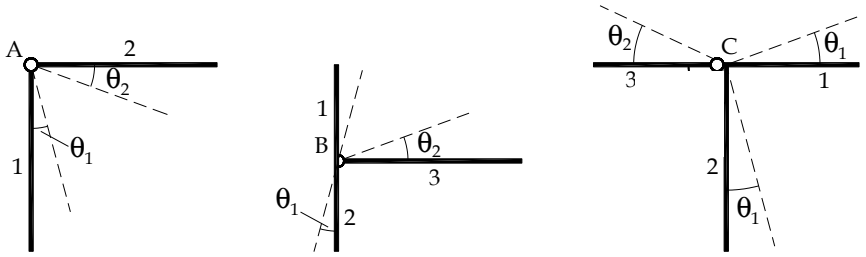


Figure 6 Some free connections and degrees of freedom numbering.

Following Figure 6 one observes that the master element defines the first rotation degree of freedom (the third of the node) and each slave element introduces an extra degree of freedom for the connection node. Figure 7 shows the introduction of elastic connections in the structures of Figure 6.

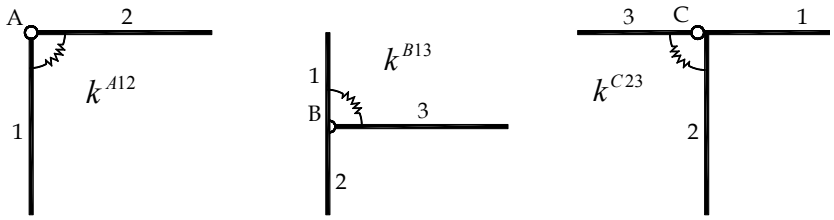


Figure 7 Some semi-rigid connections

In general, the strain energy stored in a semi-rigid connection with stiffness modulus $k^{(\eta\alpha\beta)}$ at a global node η - that is the initial (or final) node of a frame element α and the final (or initial) node of a frame element β - is given by:

$$U_\eta^{SR} = \frac{k^{(\eta\alpha\beta)}}{2}\left(\theta_\alpha^\eta - \theta_\beta^\eta\right)^2 = \frac{k^{(\eta\alpha\beta)}}{2}\left(Y_{3\alpha}^\eta - Y_{3\beta}^\eta\right)^2 \tag{33}$$

No summation implied.

3.2 Frame element strain energy:

As mentioned before the specific strain energy to be adopted here is the Saint-Venant-Kirchhoff one, that relates the Green strain ($\boldsymbol{E}$) and the second Piola-Kirchhoff stress ($\boldsymbol{S}$) in a linear way as:

$$u_e = \frac{E}{2}\left(E_{11}^2 + E_{22}^2\right) + G\left(E_{12}^2 + E_{21}^2\right) \text{ or } u_e = \frac{1}{2}\mathbf{E} : \mathfrak{C} : \mathbf{E} \tag{34}$$

in which $G = E/\left[2(1+\nu)\right]$ is the shear elastic modulus, ν is the Poisson ration and E_{ij} is the Green strain tensor. Alternatively, in dyadic notation, $\mathbf{E}$ is the Green strain tensor and $\mathfrak{C}$ is the elastic constitutive tensor. As the Green strain has been written as a function of nodal positions, see equations (16) through (28), the strain energy stored in the bar elements is written as:

$$U_e(\vec{Y}) = \int_{V_0} u_e \, dV_0 \tag{35}$$

in which V_0 is the initial volume of the analyzed structural bar elements (Coda and Greco, 2004 and Coda, 2009).

3.3 Total potential energy:

In order to write the total potential energy of the mechanical system $\Pi(\vec{Y})$ (conservative and isothermal) one sums the strain energy of frame elements, the strain energy of semi-rigid connections, the potential energy of external loads (and moments) and the potential energy of external distributed forces, resulting:

$$\Pi(\vec{Y}) = \int_{V_0} u_e(\vec{Y}) dV_0 + U_e^{SR} - \vec{F}\cdot\vec{Y} - \int_{S_0} \vec{q}\cdot\vec{y}^m(\vec{Y}) dS_0 \tag{36}$$

in which $\vec{F}$ is the external nodal force vector (including moments) and $\vec{q}$ is the general distributed force vector written as function of nodal values, by:

$$q_i = \phi_\ell(\xi) Q_{\ell i} \tag{37}$$

In equation (36), $\vec{y}^m(\vec{Y})$ is the current position at the reference line of frame elements, written as function of nodal positions $\vec{Y}$ (see equations (13) and (14)) and dS_0 is the infinitesimal length of the curved frame element.

In order to find the equilibrium configuration one applies the principium of stationary potential energy on equation (36), using as parameters the nodal positions,

$$\delta\Pi = \int_{V_0} \frac{\partial u_e}{\partial \mathbf{E}} : \frac{\partial \mathbf{E}}{\partial \vec{Y}} dV_0 \cdot \delta\vec{Y} + \frac{\partial U_e^{SR}}{\partial \vec{Y}} \cdot \delta\vec{Y} - \vec{F} \cdot \delta\vec{Y} - \int_{S_0} \vec{q} \cdot \frac{\partial \vec{y}^m}{\partial \vec{Y}} dS_0 \cdot \delta\vec{Y} = \vec{0} \tag{38}$$

By the energy conjugate principle (Ogden, 1984), the first term of the first integral of equation (38) is the second Piola-Kirchhoff stress. Using the same principle, the derivative of the strain energy stored in elastic connections is the internal moment $\vec{M}^{int}$. Therefore, in order to simplify the understanding of the physical non-linear procedure, shown in next section, one rewrites equation (38) as:

$$\delta\Pi = \int_{V_0} \mathbf{S} : \frac{\partial \mathbf{E}}{\partial \vec{Y}} dV_0 \cdot \delta\vec{Y} + \vec{M}^{int} \cdot \delta\vec{Y} - \vec{F} \cdot \delta\vec{Y} - \int_{S_0} \vec{q} \cdot \frac{\partial \vec{y}^m}{\partial \vec{Y}} dS_0 \cdot \delta\vec{Y} = \vec{0} \tag{39}$$

The understanding of equation (39) can be further improved defining the first integral as the internal nodal force and the last integral as the equivalent nodal force of applied distributed forces (Coda, 2009b), resulting:

$$\delta\Pi = \vec{F}^{int} \cdot \delta\vec{Y} + \vec{M}^{int} \cdot \delta\vec{Y} - \vec{F} \cdot \delta\vec{Y} - \mathbf{L} \cdot \vec{Q} \cdot \delta\vec{Y} = \vec{0} \tag{40}$$

in which $\mathbf{L}$ is the matrix that transforms the distributed forces into nodal equivalent ones. Due to the arbitrariness of $\delta\vec{Y}$ equation (40) results into the geometrical non-linear equilibrium equation, as:

$$\vec{F}^{int} + \vec{M}^{int} - \vec{F} - \mathbf{L} \cdot \vec{Q} = \vec{0} \tag{41}$$

The Newton-Raphson procedure is used to solve the non-linear equilibrium. This procedure is described in the next section, including the physical non-linear behavior of materials. To close this item we show the pair of internal moments, for an elastic semi-rigid connection, associated to a global node η related to the initial (or final) point of a frame element α and to the final (or initial) point of a frame element β, that is:

$$M_{3\alpha}^{\eta} = k^{(\eta\alpha\beta)} \left(Y_{3\alpha}^{\eta} - Y_{3\beta}^{\eta} \right) \text{ and } M_{3\beta}^{\eta} = -k^{(\eta\alpha\beta)} \left(Y_{3\alpha}^{\eta} - Y_{3\beta}^{\eta} \right) \tag{42}$$

4 INELASTIC PROCEDURE

4.1 Equilibrium equation

The difference between the elastic and inelastic procedures is the way the potential energy of external forces is transferred to the deformed body and dissipated during the loading process. In this case, instead of using the elastic strain energy, both for the frame element and connections, one uses the Helmholtz free energy potential (Lanczos, 1970).

Following this reasoning the total potential energy for isothermal problems is written as:

$$\Pi(\vec{Y}) = \int_{V_0} \Psi(E,\alpha)\, dV_0 + \Theta^{SR}\left(\left(Y_{3\alpha}^{\eta} - Y_{3\beta}^{\eta}\right),\bar{\alpha}\right) - \vec{F}\cdot\vec{Y} - \int_{S_0} \vec{q}\cdot\vec{y}^{m}(\vec{Y})\, dS_0 \tag{43}$$

where Ψ and Θ^{SR} are, respectively, the free energy potentials of the continuous (frame elements) and connection. These potentials are written as function of the Green strain tensor, the relative angle positions at connections and the thermodynamic parameters α and $\bar{\alpha}$.

The variation of the total potential energy is null at the equilibrium position, i.e.:

$$\delta\Pi = \int_{V_0} \frac{\partial\Psi}{\partial\mathbf{E}} : \frac{\partial\mathbf{E}}{\partial\vec{Y}}\, dV_0 \cdot \delta\vec{Y} + \frac{\partial\Theta^{molas}}{\partial\vec{Y}}\cdot\delta\vec{Y} - \vec{F}\cdot\delta\vec{Y} - \int_{S_0} \vec{q}\cdot\frac{\partial\vec{y}^{m}}{\partial\vec{Y}}\, dS_0\cdot\delta\vec{Y} = 0 \tag{44}$$

in which parameters α and $\bar{\alpha}$ are not present due to their intrinsic relation with $\boldsymbol{E}$ and $\boldsymbol{S}$ to be shown in item 4.2.

Even for inelastic problems, the derivative of the free energy potential regarding Green strain is the second Piola-Kirchhoff stress tensor. For the same reason, the energy conjugate of the free energy at elastoplastic connections regarding relative angles are internal moments. In this way, equation (44) can be written exactly as equation (39). However, with a physical non-linear meaning, i.e., while the passage from equation (38) to equation (39) is done by a simple differentiation of the quadratic potential shown by equations (31) and (33), now it is necessary to define an inelastic (plastic for instance) constitutive relation to describe the material behavior and its evolution rule.

4.2 Elastoplastic constitutive relation

In this section, we summarize the constitutive elastoplastic relation developed by Botta et al. (2008) and Rigobello et al. (2013). We follow a general 3D description in order to adequate the constitutive relation to any finite element kinematic, avoiding volumetric locking. A brief description of the main equations is given for both frame and connections.

4.2.1 Frame element

Although the developed displacements are high, the strain level present in our applications is small. Therefore, the Green strain approximates the linear strain and the second Piola-Kirchhoff stress can be used in place of the Cauchy stress. Following this reasoning we adopt the additive strain decomposition, as:

$$\boldsymbol{E} = \boldsymbol{E}^{e} + \boldsymbol{E}^{p} \text{ or } \boldsymbol{E}^{e} = \boldsymbol{E} - \boldsymbol{E}^{p} \tag{45}$$

in which $\boldsymbol{E}^{e}$ and $\boldsymbol{E}^{p}$ are, respectively, the elastic and plastic parts of $\boldsymbol{E}$. Therefore, the free energy potential can be written as:

$$\Psi(\boldsymbol{E}-\boldsymbol{E}^p,\alpha)=\frac{1}{2}\boldsymbol{E}^e:\mathfrak{C}:\boldsymbol{E}^e+\frac{1}{2}h\alpha^2 \tag{46}$$

where $\mathfrak{C}$ is the elastic constitutive tensor and h is the isotropic hardening parameter.

The second Piola-Kirchhoff stress and the thermodynamic force χ are written as:

$$\boldsymbol{S}=\frac{\partial\Psi}{\partial\boldsymbol{E}}=\mathfrak{C}:\boldsymbol{E}^e=\mathfrak{C}:\left(\boldsymbol{E}-\boldsymbol{E}^p\right) \tag{47}$$

$$\chi=-\frac{\partial\Psi}{\partial\alpha}=-h\alpha \tag{48}$$

As mentioned after equation (44), in order to eliminate α from equilibrium equation it is necessary to relate $\boldsymbol{E}^p$ and α. In classical formulations this is done introducing a plastic potential $F\left(\boldsymbol{S},\chi\right)$ (Simo and Hughes, 1998) for which the plastic flow is given by:

$$\dot{\boldsymbol{E}}^p=\dot{\lambda}\frac{\partial F}{\partial\boldsymbol{S}} \quad \text{and} \quad \dot{\alpha}=\dot{\lambda}\frac{\partial F}{\partial\chi} \tag{49}$$

or in infinitesimal notation:

$$d\boldsymbol{E}^p=d\lambda\frac{\partial F}{\partial\boldsymbol{S}} \quad \text{and} \quad d\alpha=d\lambda\frac{\partial F}{\partial\chi} \tag{50}$$

where λ is the plastic multiplier. In the adopted formulation (Botta et al., 2008 and Rigobello et al., 2013) equations (48) and (50) are replaced by $\alpha=-\lambda$ and:

$$d\boldsymbol{E}^p=\boldsymbol{\eta}\,d\lambda \quad \text{and} \quad d\chi=h\,d\lambda \tag{51}$$

for which,

$$\boldsymbol{\eta}=\mathfrak{D}^p:\boldsymbol{S}=\frac{G}{\sqrt{J_2}}\left(\frac{\bar{\boldsymbol{S}}}{2G}+\frac{tr\left(\boldsymbol{S}\right)}{9k^p}\boldsymbol{I}\right) \quad \text{and} \quad \mathfrak{D}^p=\frac{G}{\sqrt{J_2}}\left(\mathfrak{C}^p\right)^{-1} \tag{52}$$

in which $J_2=1/2\left[\bar{\boldsymbol{S}}:\bar{\boldsymbol{S}}^t\right]$ is the second invariant of the deviatory stress $\bar{\boldsymbol{S}}$ and $\mathfrak{C}^p$ is an elastic constitutive tensor, similar to $\mathfrak{C}$ changing the ν by ν^p. Moreover $k^p=E/\left[3\left(1-2\nu^p\right)\right]$ is the elastoplastic bulk modulus. Following this strategy, when $\nu^p\cong 0.5$ isochoric plasticity takes place

and when $\boldsymbol{\nu} = \boldsymbol{\nu}^p$ the plastic flow occurs in the same direction of elastic flow. In this work we adopt $\mathfrak{C}^p = \mathfrak{C}$, defined by the second derivative of expression (34) regarding strain. This choice releases any possible locking related to Reissner kinematic.

To complete the elastoplastic procedure one defines the yielding failure expression as:

$$f = \sqrt{J_2} - \chi - S_y \tag{53}$$

in which $S_y = \sigma_y / \sqrt{3}$ is the initial size of the Von-Mises surface ($f = 0$) with σ_y being the yielding uniaxial stress.

It is important to know that the plastic multiplier should satisfy the Khun-Tucker conditions, related to the yielding surface (53), i.e.:

$$d\lambda \geq 0\,,\ f \leq 0\,,\ d\lambda\, f = 0 \tag{54}$$

which means that if $f \leq 0$ then $d\lambda = 0$ and no plastic evolution occurs and if, for some situation, one finds $f > 0$ then $d\lambda \geq 0$ should be achieved in order to guaranty the equality $f = 0$.

In terms of incremental solution we assume constant by parts hardening (h) and a typical interval $\left[t_n, t_{n+1}\right]$ for which n is a previous (solved) step and $n+1$ is the current step. Therefore, one writes:

${}^t\boldsymbol{E}_{(n+1)}$	$\rightarrow$	Elastic trial of the total strain
${}^t\boldsymbol{E}^p_{(n+1)} = \boldsymbol{E}^p_n$	$\rightarrow$	Accumulated plastic strain (assumed as trial)
${}^t\lambda_{(n+1)} = \lambda_n$	$\rightarrow$	Internal variable trial
${}^t\chi_{(n+1)} = \chi_n$	$\rightarrow$	Thermodynamic internal force trial

Using these variables we calculate the stress level considering $\Delta\boldsymbol{E}^p$ (instead of $d\boldsymbol{E}^p$) as the main unknown, as follows

$$\boldsymbol{S}_{(n+1)} = \mathfrak{C} : \left({}^t\boldsymbol{E}_{(n+1)} - {}^t\boldsymbol{E}^p_n - \Delta\boldsymbol{E}^p \right) = {}^t\boldsymbol{S}_{(n+1)} - \mathfrak{C} : \Delta\boldsymbol{E}^p \tag{55}$$

where the trial stress ${}^t\boldsymbol{S}$ is known. Using this value we calculate the trial yielding expression:

$${}^t f_{(n+1)} = \sqrt{{}^t J_2} - {}^t\chi - S_y \tag{56}$$

If ${}^{t}f_{(n+1)} \leq 0$ the step is elastic and the trial variables are the correct ones. However, if ${}^{t}f_{(n+1)} > 0$ then the step is elastoplastic and $f_{(n+1)}$ should assume zero, resulting:

$$\Delta\lambda = {}^{t}f_{(n+1)} / \left(G + H\right) \tag{57}$$

Finally, using equations (51) and (52), the searched plastic strain is found as,

$$\Delta \boldsymbol{E}^{P} = \frac{{}^{t}f_{(n+1)}}{\left(G+H\right)}\left(\frac{{}^{t}\bar{\boldsymbol{S}}_{(n+1)}}{2\sqrt{{}^{t}J_{2(n+1)}}} + \frac{G\,tr\left({}^{t}\boldsymbol{S}\right)}{9k^{P}\sqrt{{}^{t}J_{2(n+1)}}}\mathbf{I} \right) \tag{58}$$

Moreover, the elastoplastic constitutive tensor is written as (Rigobello et al., 2013):

$$\mathfrak{C}^{ep} = \frac{\partial \mathbf{S}}{\partial \mathbf{E}} = \frac{\partial^2 \Psi}{\partial \mathbf{E}\,\partial \mathbf{E}} = \mathfrak{C} - \left(\frac{\mathfrak{C} : \boldsymbol{\eta} \otimes {}^{t}\bar{\boldsymbol{S}} : \mathfrak{C}}{{}^{t}\bar{\boldsymbol{S}} : \mathfrak{C} : \boldsymbol{\eta} + 2\sqrt{J_2}H} \right) = \mathfrak{C} - \mathfrak{C}^{p} \tag{59}$$

4.2.2 Elastoplastic model for the semi-rigid connections

In this item the previous general elastoplastic procedure (multi-linear) is simplified to accomplish the semi-rigid connection. Firstly, the notation of equations (33) and (42) is changed to:

$$R^{\eta}_{3\alpha\beta} = \left(Y^{\eta}_{3\alpha} - Y^{\eta}_{3\beta} \right) \tag{60}$$

where $R^{\eta}_{3\alpha\beta}$ is the relative rotation between frame bars α and β at a connection node η. From now on, to simplify the developments, this relative rotation will be called simply R. This variable is clearly one-dimensional and is separated into elastic and plastic parts, as:

$$R = R^{e} + R^{p} \quad \text{or} \quad R^{e} = R - R^{p} \tag{61}$$

The free Helmholtz energy potential, implicit in equation (43), is written as:

$$\Theta^{SR}(R - R^{p}, \bar{\alpha}) = \frac{1}{2}k(R^{e})^{2} + \frac{1}{2}h\bar{\alpha}^{2} \tag{62}$$

where k is the elastic stiffness of the connection and h its hardening. Using the work of Botta et al. (2008) and Rigobello et al. (2013) and following the previous item one writes the internal moment and the thermodynamic force related to the internal variable $\bar{\alpha}$ as:

$$M = \frac{\partial \Theta^{SR}}{\partial R} = kR^e = k(R - R^p) \tag{63}$$

$$\chi = -\frac{\partial \theta}{\partial \bar{\alpha}} = -h\bar{\alpha} \tag{64}$$

In the case of semi-rigid connections, the elastic limiting moment $M_y > 0$ is used to write the failure expression as:

$$f = \left|M\right| - M_y - \chi \le 0 \quad \text{or} \quad f = \left|M\right| - M_y + h\bar{\alpha} \le 0 \tag{65}$$

in which isotropic hardening is adopted.

Following the steps described in the previous item, one achieves:

$$\Delta R^p = sign(M).\frac{{}^t f}{k+h} \tag{66}$$

in which $sign$ represents signal. Moreover the tangent modulus results:

$$k_t = \frac{\partial^2 \Theta^{SR}}{\partial R^2} = \frac{k.h}{k+h} \tag{67}$$

5 Newton-Raphson procedure

Knowing the elastoplastic constitutive models, one starts the solution process rewriting the equilibrium equation (44) as:

$$\vec{g}(\vec{Y}) = \int_{V_0} \frac{\partial \Psi}{\partial \mathbf{E}} : \frac{\partial \mathbf{E}}{\partial \vec{Y}} dV_0 + \frac{\partial \Theta^{SR}}{\partial \vec{Y}} - \vec{F} - \int_{S_0} \vec{q} \cdot \frac{\partial \vec{y}^m}{\partial \vec{Y}} dS_0 = \vec{0} \tag{68}$$

Remembering that the process is nonlinear, equation (68) is expanded in Taylor series from a trial position $\vec{Y}_0$, i.e.:

$$\vec{g}(\vec{Y}) \cong \vec{g}(\vec{Y}_0) + \left.\frac{\partial \vec{g}}{\partial \vec{Y}}\right|_{\vec{Y}_0} \Delta\vec{Y} = \vec{0} \tag{69}$$

Solving the linear system of equation (69) one finds the position correction $\Delta\vec{Y}$, applied as $\vec{Y} = \vec{Y} + \Delta\vec{Y}$ until $\left|\Delta\vec{Y}\right| / \left|\vec{X}\right| < tol$, in which tol is the tolerance in positions and $\vec{X}$ is the initial

nodal positions of the body. As the applied forces are conservative the derivative of $\vec{g}$ regarding positions results:

$$\frac{\partial \vec{g}}{\partial \vec{Y}} = \left(\frac{\partial \mathbf{E}}{\partial \vec{Y}} : \frac{\partial^2 \Psi}{\partial \mathbf{E} \partial \mathbf{E}} : \frac{\partial \mathbf{E}}{\partial \vec{Y}} + \mathbf{S} : \frac{\partial^2 \mathbf{E}}{\partial \vec{Y}\, \partial \vec{Y}} \right) + \frac{\partial^2 \Theta}{\partial \vec{Y}\, \partial \vec{Y}} \tag{70}$$

or, using equations (59) and (67),

$$\frac{\partial \vec{g}}{\partial \vec{Y}} = \left(\frac{\partial \mathbf{E}}{\partial \vec{Y}} : \mathfrak{C}^{ep} : \frac{\partial \mathbf{E}}{\partial \vec{Y}} + \mathbf{S} : \frac{\partial^2 \mathbf{E}}{\partial \vec{Y}\, \partial \vec{Y}} \right) + K_t \tag{71}$$

The derivatives of the Green strain regarding positions are straightforward and left to the reader.

6 EXAMPLES

6.1 Elastoplastic connection of two bars

This example is used to confirm the computational implementation of the elastoplastic connection, to demonstrate the geometrically exact description of the proposed total Lagrangian frame formulation and to describe the difference of non-linear elastic and elastoplastic connection models.

A clamped bar is divided into two equal elastic parts linked by an elastoplastic connection, as seen in Figure 8.

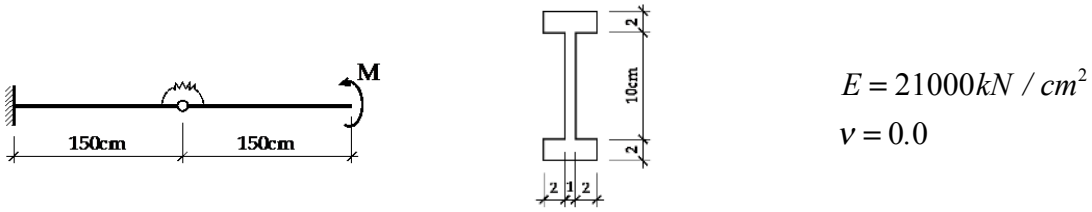
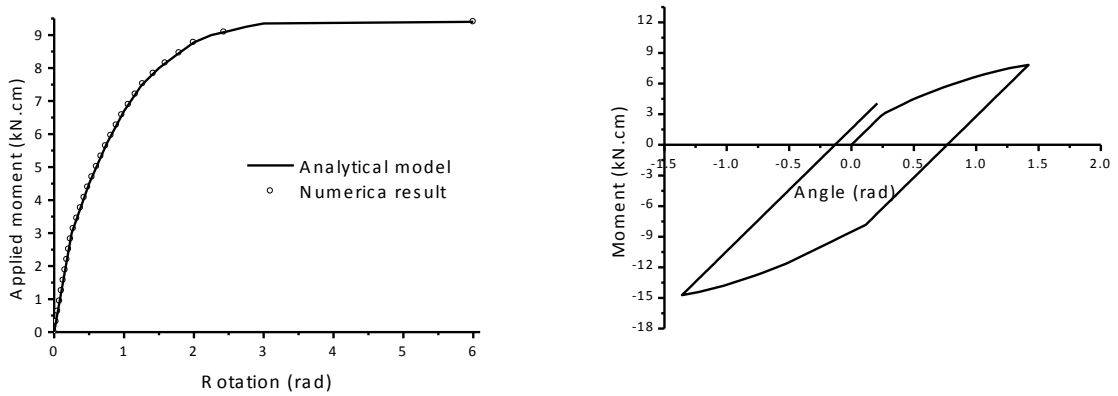


Figure 8 Clamped bar connected by an elastoplastic connection

The cross section and the elastic properties of the bar are also depicted in Figure 8. Two finite elements of cubic approximation order have been used and the load is divided into 30 steps. Figure 9a shows the moment versus rotation graphic comparing the numerical result with the analytical curve for a monotonically crescent load. The initial elastic modulus of the connection is $k = 12kN.cm$ with elastic limit $M_y = 3kN.cm$. Figure 9b shows the connection behavior when subjected to a cyclic loading.

As one can see in Figure 9 the formulation models perfectly the elastoplastic connection behavior; highlighting that the multi-linear strategy is capable of accurately reproduce any elastoplastic curve. It is important to mention that if one uses a non-linear elastic model, as the ones adopted,

for example, by Pinheiro and Silveira (2005) and Chan and Chui (2000), the loading situation (Figure 9a) will present the same result as the analytical solution; however their models are unable to reproduce the real unloading or cycling situation (Figure 9b), that is, in their formulation no plastic evolution takes place and the unloading follows the same curve as loading, which results into no plastic residuals at a new resting position.



(a) Monotonic loading (b) Cycling loading

Figure 9 Connection moment x rotation graphics – a) Monotonic, b) Cyclic.

Figure 10 shows partial positions for 15 equally spaced loading levels demonstrating that the non-linear geometric description is exact. This level of rotation is not accomplished by formulations that adopt second order geometrical descriptions.

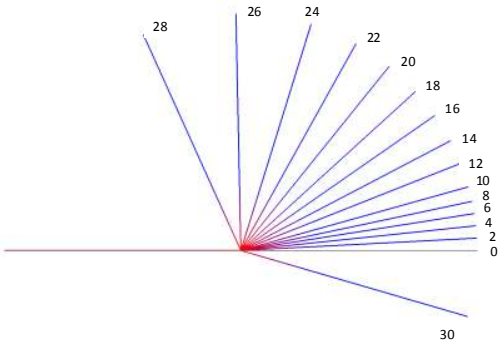


Figure 10 Partial positions for equally spaced loads

6.2 Four point test

A simple supported beam, subjected to a monotonically crescent controlled displacement at load positions, see Figure 11, is analyzed. The cross section is also presented in Figure 11, for which three lamina are employed to perform the Gauss integration procedure. Five Gauss integration points are adopted for each lamina. Two different materials are employed for comparisons, one is

perfect elastoplastic and the other presents softening, see Figure 12a.

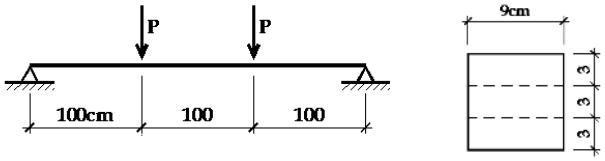
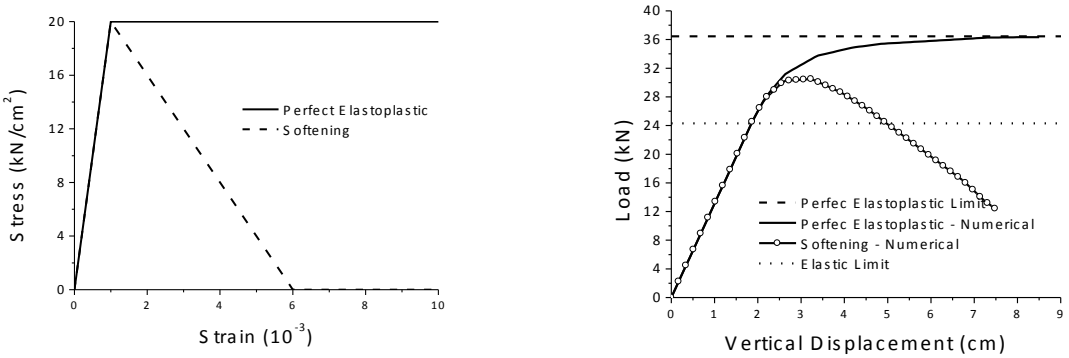


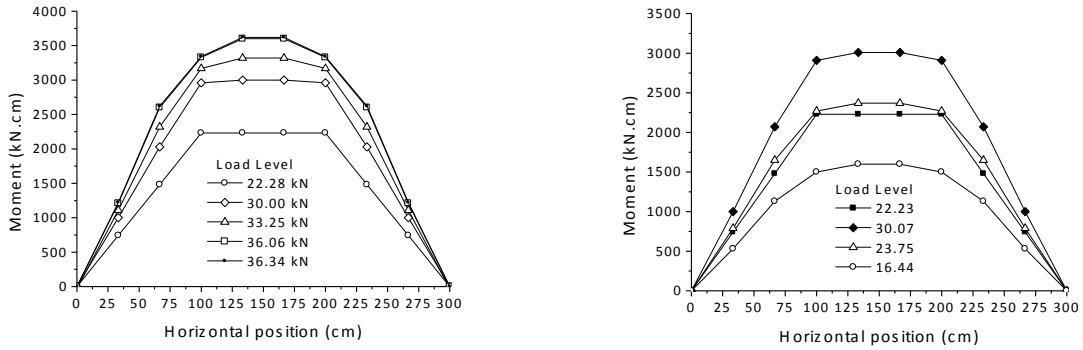
Figure 11 Simple supported beam - loading and cross section



(a) Stress-strain relation (b) Load versus displacement

Figure 12 Curves: stress x strain and force x displacement (under the load)

Figure 12b shows the beam behavior for both materials. Results are compared to the elastic limit load and the ultimate load for perfect elastoplasticity. Position control is sufficient to model the post critical behavior of this example. Three cubic elements (without considering symmetry) are used to model this case.



(a) Perfect elastoplastic (b) Softening

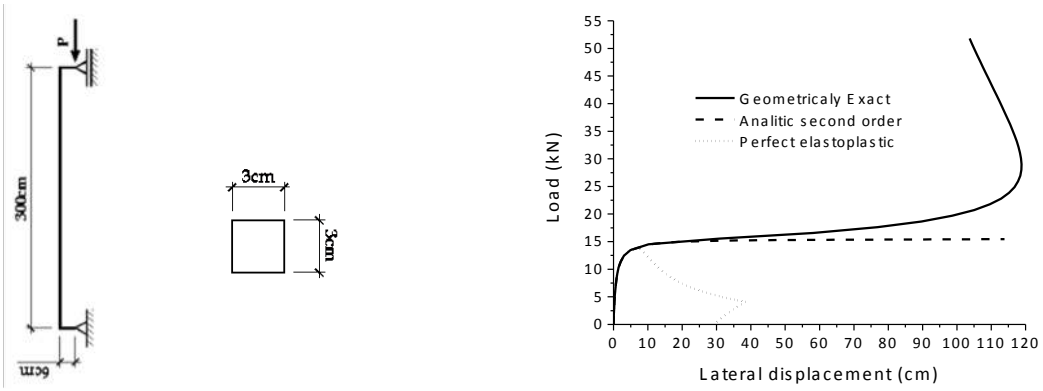
Figure 13 Bending moments diagrams for various load levels

Figure 13 shows the evolution of bending moments for different load levels. One can observe that for the perfect elastoplastic case the degradation spread over the beam; moreover the load stabilizes after the displacement of 7cm. For the material that presents softening, after the imposed displace-

ment of 2.2cm a reduction in the load level occurs for crescent imposed displacements and, consequently, in the bending moment. Moreover, no bending moment spreads over the beam.

6.3 Elastoplastic column

This example illustrates the application of the proposed formulation to the eccentric compression of the column depicted in Figure 14a. The material properties are: $E = 21000kN/cm^2$, $\nu = 0.0$ and $\sigma_y = 21kN/cm^2$ with perfect elastoplasticity. Figure 14b shows the results obtained using the proposed formulation (geometrically exact) for the elastic and elastoplastic cases. These solutions are compared to the elastic closed second order analytical solution (secant formulae). We adopt six cubic finite elements to run this example, four along the column and two for the small consoles at extremities. Position control is employed and, to impose symmetry, the rotation of the central node is restricted.



(a) Geometry (b) Load versus central displacement

Figure 14 Eccentric column and results.

This example confirms that the elastic second order theory gives a more flexible result than the elastic geometrically exact one. The plastic flow starts at the load level of $13kN$, 16% less than the column critical load ($15.545kN$). The elastic release starts at the load level $3.773kN$ and the residual displacement, at the new unloaded situation, is about $30cm$.

6.4 Frame analysis subjected to concentrated loads - Elastoplastic connection

In this example the frames depicted in Figure 15 are analyzed considering elastoplastic connections. The original data of this problem are given by Pinheiro and Silveira (2005) and Chan and Chui (2000). In these works the connection model does not consider plasticity, the geometry follows the second order approximation and the kinematic does not include shear effects. To simplify comparisons, we adopt elastic bars with $E = 21000kN/cm^2$ and $\nu = 0.0$.

The adopted multi-linear connection diagrams, shown in Figure 16, are extracted from Pinheiro and Silveira (2005). The elastic limits of the connections for the four tested cases are:

$M_y^A = 750kN.cm$, $M_y^B = 1625kN.cm$, $M_y^C = 5000kN.cm$ and $M_y^D = 20480kN.cm$ with their corresponding rotations $\theta_y^A = 1.67x10^{-3}\,rad$, $\theta_y^B = 1.67x10^{-3}\,rad$, $\theta_y^C = 5.00x10^{-3}\,rad$ and $\theta_y^D = 6.67x10^{-3}\,rad$. More data information can be seen in Pinheiro and Silveira (2005).

Beams are constituted of steel wide flange shaped section $W14x48$ while columns are constituted of $W12x96$ section. It is interesting to note that bars behave elastically because the ultimate limit of the strongest connection (case D) is practically equal to the elastic limit of beams, and loads are applied at connections.

The load P (Figure 15) grows monotonically until the critical load shows up. Figures 17 and 18 show that the results presented by our formulation agree with the ones given by references. For semi-rigid connections the differences in results are less the 2% for all cases. For rigid connection the difference is about 6%, explained by the difference among the exact geometrical description and second order approximation.

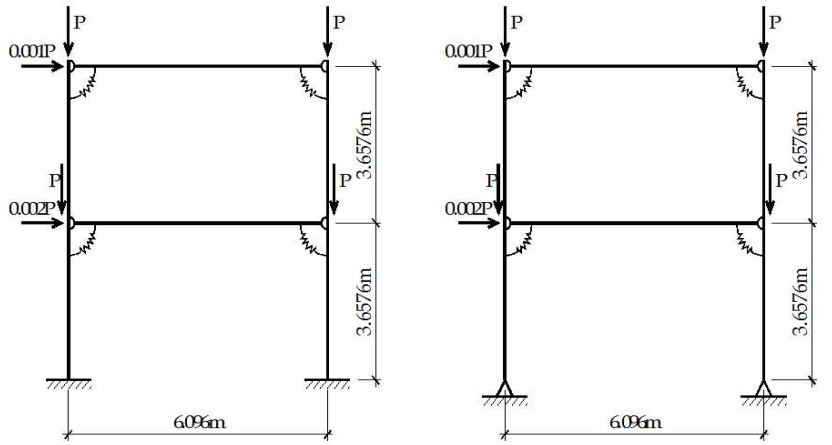


Figure 15 Analized frames, adapted from Pinheiro and Silveira (2005)

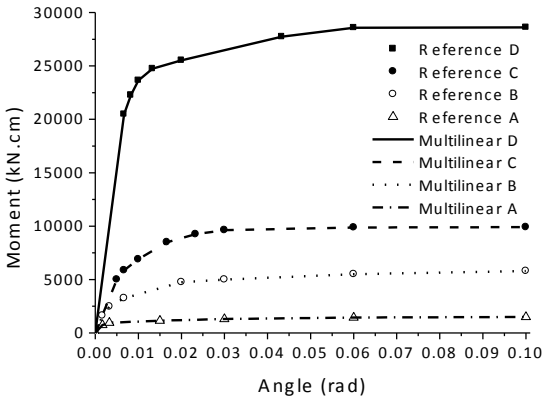


Figure 16 Connections bending moment x rotation diagrams

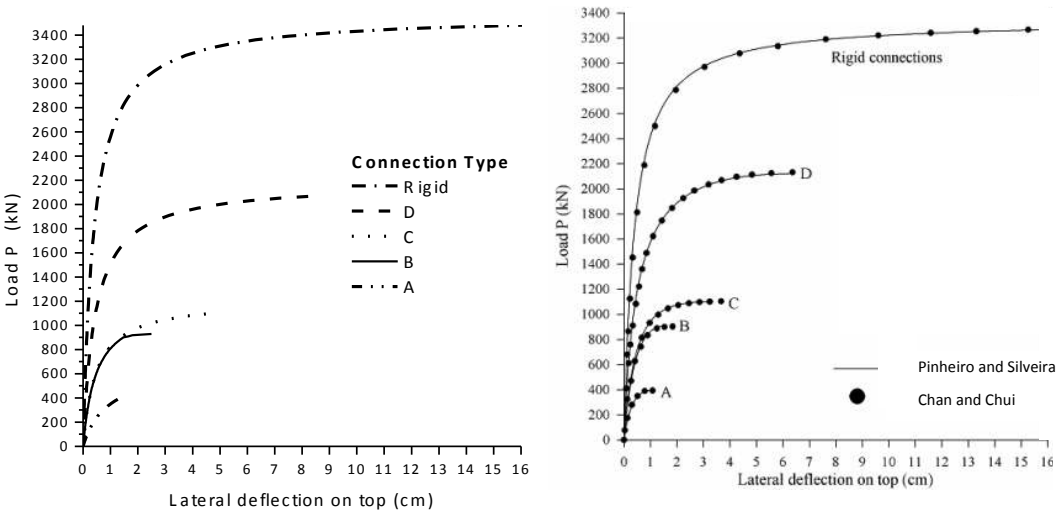


Figure 17 Simple supported structure behavior

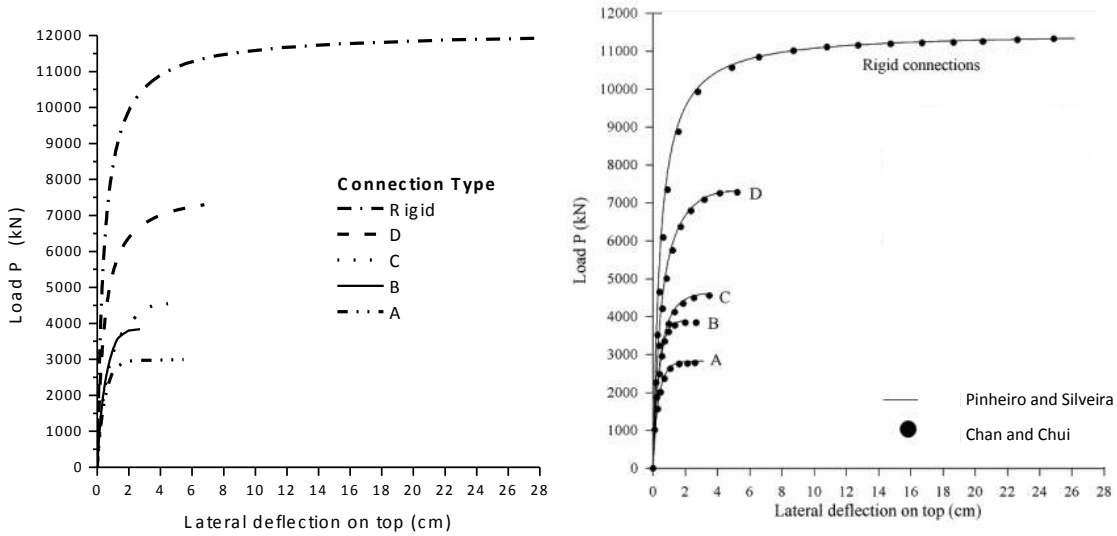


Figure 18 Clamped structure behavior

For connections A and B the displacement levels are very small and failure occurs in an abrupt way. In order to show up the horizontal plateau (for A and B), Figures 17 and 18, we used lateral loads of $0.0015P$ and $0.003P$ instead of $0.001P$ and $0.002P$. However, this procedure does not change the critical load value.

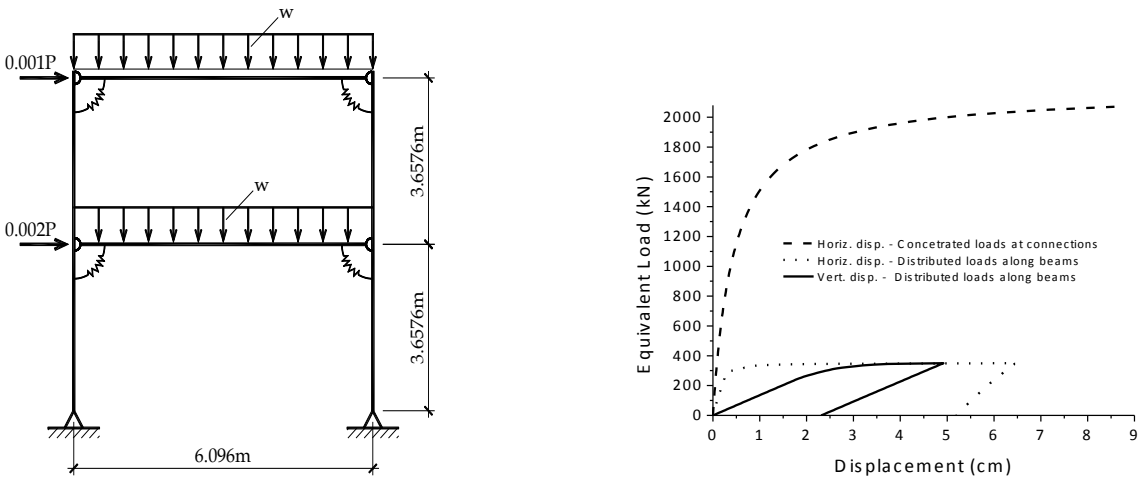
6.5 Frame analysis subjected to distributed loads - Elastoplastic connection

A change in the last example is introduced in order to compare the structure behavior when the same load is applied distributed along beams or concentrated at connections. As the analysis includes an unload situation it cannot be done using formulations that consider elastic frame elements and non-linear elastic connections.

Vertical and horizontal loads are depicted in Figure 19a. The frame is simple supported and the connections are of type D. The physical parameters to model the frame bars are $E = 21000kN/cm^2$, $\nu = 0.0$ and $\sigma_y = 21kN/cm^2$ (perfect elastoplasticity). Cross sections are the same ones employed in example 6.4, i.e., $W14x48$ for beams and $W12x96$ for columns.

Figure 19b presents the horizontal displacement at the top of the structure for concentrated (at connections) and distributed (along beams) vertical loads. Figure 19b also shows the vertical displacement at the center of the top beam for the case of distributed loading. The load equivalence is given by $P = wL/2$, in which w is the distributed load, see Figure 19a. The distributed load level grows until the imminence of failure then the structure is unloaded.

From Figure 19b, the application of distributed load, instead of concentrated ones, leads to the yielding of horizontal elements. As a consequence there is a loss of overall flexural stiffness resulting into a smaller critical load when compared to the concentrated loading case. Moreover, the unloading reveals the presence of residual plastic strain for the applied load level.



(a) Analyzed structure ans loading (b) Results

Figure 19 Analyzed structure and results

7 CONCLUSIONS

In this work an alternative FEM formulation based on positions to the analysis of geometrical and physical non-linear behavior of structures is proposed and implemented. The geometrical description is exact and the kinematics considers shear stress in the energy and failure calculations. The cross sections are laminated and enable physical non-linear calculations with the required precision. Semi-rigid elastoplastic connections are developed and implemented. The elastoplastic behavior of connections and bars are multi-linear and enables the accurate reproduction of any stress-strain experimental behavior. Moreover, closed solutions are given to the plastic multipliers improving the efficiency of the proposed technique.

Examples show the formulation capacity in modeling structures that present large displacements and rotations, as well as, the accuracy in modeling continuous elements developing plasticity. Critical load level can also be achieved using the proposed methodology, as shown at specific examples.

Acknowledgments *Authors would like to thanks FAPESP (São Paulo research foundation) and CNPq (National Council for Scientific and Technological Development - Brazil) for the financial support of this research.*

References

Abdalla K.M. and Chen W.F. (1995), Expanded database of semi-rigid steel connections. Comp. Struct., 56(4):553-564.

Alvarenga AR, Silveira RAM. (2009), Second-order plastic-zone analysis of steel frames Part I: Numerical formulation and examples of validation. Lat Am J Solids Stru; 6:323 – 342.

Ang K.M. and Morris G.A.(1984), Analysis of three-dimensional frames with °exible beam-column connections. Can. J. Civil Eng., 11:245-254.

Argyris J. H., Boni B., Hindenlang U., and Kleiber M. (1982), Finite element analysis of two- and three-dimensional elasto-plastic frames-the natural approach, Computer Methods in Applied Mechanics and Engineering, 35 (2), no. 2, pp. 221–248.

Armero F. and Ehrlich D. (2006), Numerical modeling of softening hinges in thin Euler-Bernoulli beams, Computers & Structures, 84 (10-11), 641–656

Avery P, Mahendran M. (2000), Distributed plasticity analysis of steel frame structures comprising non-compact sections. Eng Struct; 22:901-919.

Bonet J., Wood R.D., Mahaney J., Heywood P. (2000), "Finite element analysis of air supported membrane structures" Computer Methods in Applied Mechanics and Engineering, 190 (5-7), 579-595.

Botta A.S., Paccola R.R., Venturini W.S., Coda H.B. (2008), "A discussion on volume change in the plastic phase", Commun. Numer. Meth. En., 24, 1149–1162.

Chan S.L., and Chui, P.P.T. (2000), "Nonlinear Static and Cyclic Analysis of Steel Frames with Semi-Rigid Connections", Elsevier, Oxford.

Chan S.L., Zhou Z.H. (2004), "Elastoplastic and large deflection analysis of steel frames by one element per member. II: Three hinges along member", J Struct Eng-ASCE, 130, 545– 553.

Chen W.F. and Kishi N. (1998). Semi-rigid steel beam-to-column connections: Data base and modeling. J. Struct. Div. ASCE, 115(1):105{119, 1989.

Chen WF, Goto Y, Liew JYR. (1996), Stability design of semi-rigid frames. John Wiley & Sons.

Chiorean C.G., Barsan G.M. (2005), "Large deflection distributed plasticity analysis of 3D steel frameworks", Comp & Struct, 83, 1555–1571.

Chui P. P. T. and Chan S. L., (1997), Vibration and de°ection characteristics of semi-rigid jointed frames. Engineering Structures, 19(12):1001-1010.

Coda, H.B. (2009a) "A solid-like FEM for geometrically non-linear 3D frames", Computer Methods in Applied Mechanics and Engineering, 198 (47-48), 3712-3722.

Coda, H.B. (2009), "Two dimensional analysis of inflatable structures by the positional FEM", Latin American Journal of Solids and Structures, 6 (3), 187-212

Coda H.B.; Greco M. (2004), "A simple FEM formulation for large deflection 2D frame analysis based on position description" Computer Methods in Applied Mechanics and Engineering, 193 (33-35), 3541-3557.

Coda H.B., Paccola R.R. (2007), "An alternative positional FEM formulation for geometrically nonlinear analysis of shells: Curved triangular isoparametric elements", Computational Mechanics, 40 (1), 185-200.

Coda, H.B. and Paccola, R.R., (2008), "A positional FEM Formulation for geometrical non-linear analysis of shells", Latin American Journal of Solids and Structures 5 (3), 205-223.

Coda H.B.; Paccola R.R. (2010), "Improved finite element for 3D laminate frame analysis including warping for any cross-section", Applied Mathematical Modelling 34 (4), 1107-1137.

Coda H.B.; Paccola R.R. (2011), "A FEM procedure based on positions and unconstrained vectors applied to non-linear dynamic of 3D frames", Finite Elements in Analysis and Design, 42 (4), 319-333.

Ehrlich D. and Armero F. (2005), Finite element methods for the analysis of softening plastic hinges in beams and frames, Computational Mechanics, 35 (4), pp. 237–264.

Frye M.J. and Morris G.A. (1975), Analysis of °exibly connected steel frames. Can. J. Civil Eng., 2(3):280-291.

Gruttmann F, Sauer R, Wagner W. (2000) Theory and numerics of three-dimensional beams with elastoplastic material behavior. Int J Numer Meth Engng; 48:1675-1702.

Kim, S.E, Lee D.H. (2002), "Second-order distributed plasticity analysis of space steel frames". Eng Struct, 24 (6), 735–44.

King. W. S. (1994) The limit loads of steel semi-rigid frames analyzed with different methods. Computers and Structures, 51(5):475-487.

Kishi N. and Chen W. F. (1986a), Steel Connection Data Bank Program. Structural Engineering Report No. CE-STR-86-18. School of Civil Engineering, Purdue Univ., West Lafayette, IN.

Kishi N. and Chen W. F. (1986b), Data Base of Steel Beam-to-Column Connections. Structural Engineering Report No. CE-STR-93-15. School of Civil Engineering, Purdue Univ., West Lafayette, IN.

Kruger T. S., van Rensburg B. W. J., and du Plessis G. M. (1995), Nonlinear analysis of structural steel

frames. J. Construct. Steel Research, (34):285-306.

Lanczos C. (1970), "The variacional principles of mechanics", Dover, New York, fourth edition.

Landesmann A, Batista EM. (2005), Advanced analysis of steel framed buildings to brazilian standard and Eurocode–3. J Constr Steel Res. 61:1051–1074.

Lui E.M. and Chen W. F. (1986), Analysis and behavior of °exibly jointed frames. Engineering Structures, 8:107-118.

Lui E. M. and Chen W. F. (1988), Behavior of braced and unbraced semi-rigid frames. International Journal of Solids Structures, 24(9):893-913.

Ngo-Hu C., Kim S.E, Oh, J.R. (2007), "Nonlinear analysis of space steel Frames using fiber plastic hinge concept", Eng Struct, 29, 649–657.

Nogueira C.G., Venturini W.S., Coda H.B., (2013), Material and geometric nonlinear analysis of reinforced concrete frame structures considering the influence of shear strength complementary mechanisms, Latin American Journal of Solids and Structures, 10 (5), 953-980.

Ogden R.W. (1984), Non-linear Elastic deformation, Ellis Horwood, England.

Pascon J.P, Coda H.B. (2013), A shell finite element formulation to analyze highly deformable rubber-like materials, Latin American Journal of Solids and Structures, 10 (6), 1177-1209.

Pinheiro L. (2003), Non-Linear Analysis of Spatial Truss and Plane Frames with Semi-Rigid Connections, M.Sc. Thesis. PROPEC/Deciv/School of Mines, UFOP (in Portuguese).

Pinheiro L., and Silveira, R.A.M. (2005), "Computational procedures for nonlinear analysis of frames with semi-rigid connections", Latin Am. Journal of Solids and Structures, 2, 339-367.

Silva W.Q., Coda H.B., (2012), Numerical combination for nonlinear analysis of structures coupled to layered soils, Latin American Journal of Solids and Structures, 9 (2), 235-257.

Simo J.C., Hughes T.J.R. (1998), Computational Inelasticity, Springer.

Sekulovic M. and Salatic R.. (2001), Nonlinear analysis of frames with °exible connections. Computers and Structures, 79(11):1097-1107.

Simões L. M. C. (1996), Optimization of frames with semi-rigid connections. Computers and Structures, 60(4):531-539.

Ren, WX; Tan, XG; Zheng, ZC. (1999), Nonlinear analysis of plane frames using rigid body-spring discrete element method, COMPUTERS & STRUCTURES, 71 (1), 105-119.

Richard R.M. and Abbott B.J. (1975), Versatile elastic-plastic stress-strain formula. Journal of Engineering Mechanics, Div. ASCE, 101(4):511-515.

Rigobello, Ronaldo; Coda, Humberto Breves; Neto, Jorge Munaiar, (2013), Inelastic analysis of steel frames with a solid-like finite element, JOURNAL OF CONSTRUCTIONAL STEEL RESEARCH, 86, pp. 140-152.

White DW. (1993), Plastic hinge methods for advanced analysis of steel frames. J Constr Steel Res.; 24(2):121–52.

Xu L. (2001) Second-order analysis for semi-rigid steel frame design. Canadian Journal of Civil Engineering, (28):59-76, 2001.

Zhou, ZH; Chan, SL. (2004), Elastoplastic and large deflection analysis of steel frames by one element per member. I: One hinge along member JOURNAL OF STRUCTURAL ENGINEERING-ASCE, 130 (4), 538-544

Zhu K., Al-Bermani F.G.A., Kitipornchai S., and Li B. (1995), Dynamic response of °exibility jointed frames. J. Struct. Div. ASCE, 17(8):575-580.